

Observational Properties of SNe Ia Progenitors Close to the Explosion

A. Tornambé,^{1*} L. Piersanti,^{2,3} G. Raimondo,² R. Delgrande^{4,5,1}

¹INAF-Osservatorio Astronomico di Roma, via Frascati, 33, I-00040, Monte Porzio Catone, Italy

²INAF-Osservatorio Astronomico d'Abruzzo, via Mentore Maggini, snc, I-64100, Teramo, Italy

³INFN-Sezione di Perugia, via A. Pascoli, I-06123 Perugia, Italy

⁴Physics Department, Università di Roma “Tor Vergata”, via della Ricerca Scientifica, 1, I-00133, Roma, Italy

⁵ INFN-LNF, via E. Fermi 40, I-00044, Frascati, Italy

Accepted XXX. Received YYY; in original form ZZZ

ABSTRACT

We determine the expected signal in various observational bands of Supernovae Ia progenitors just before the explosion by assuming the rotating Double Degenerate scenario. Our results are valid also for all the evolutionary scenarios invoking rotation as the driving mechanism of the accretion process as well as the evolution up to the explosion. We find that the observational properties depend mainly on the mass of the exploding object, even if the angular momentum evolution after the end of the mass accretion phase and before the onset of C-burning plays a non-negligible role. Just before the explosion the magnitude M_V ranges between 9 and 11 mag, while the colour (F225W-F555W) is about -1.64 mag. The photometric properties remain constant for a few decades before the explosion. During the last few months the luminosity decreases very rapidly. The corresponding decline in the optical bands varies from few hundredths up to one magnitude, the exact value depending on both the WD total mass and the braking efficiency at the end of the mass transfer. This feature is related to the exponentially increasing energy production which drives the formation of a convective core rapidly extending over a large part of the exploding object. Also a drop in the angular velocity occurs. We find that observations in the soft X band (0.5–2 keV) may be used to check if the SNe Ia progenitors evolution up to explosion is driven by rotation and, hence, to discriminate among different progenitor scenarios.

Key words: Binaries: general — Supernovae: general

1 INTRODUCTION

In spite of their pivotal role in observational cosmology, type Ia Supernovae (SNe Ia) still remain an intriguing mystery, as no clear consensus about their progenitor system exists so far. In fact, the observational properties of the resulting explosive event are largely independent of the considered scenario for the progenitor’s explosion, mainly because the explosion itself smears out almost completely the previous evolutionary imprint. It has been suggested that some indications about the progenitors could be derived by analyzing archival images of the site where a SN Ia explodes (e.g. Li et al. 2011; Kelly et al. 2014; McCully et al. 2014). We note that the imprint of the progenitor could be found

either if the donor star is still there at the epoch of the explosion, as expected in the classical Single Degenerate (SD) scenario (Whelan & Iben 1973), or some material coming from the donor remains in the circumstellar medium, as is possible in the classical Double Degenerate (DD) scenario (Iben & Tutukov 1984). In recent years, it has been suggested that rotation plays a major role in determining the evolution up to the explosion (Piersanti et al. 2003a,b; Di Stefano et al. 2011; Hachisu et al. 2012). In fact, in interacting binary systems the accretor may acquire a large rotational velocity owing to the continuous angular momentum deposition via mass transfer. Rotation overcomes many shortcomings of both the SD and DD scenarios; in addition it represents a key ingredient in the Core Degenerate (CD) scenario by Ilkov & Soker (2012). Since rotation “lifts” stellar structures, it transpires that rotating objects can increase their total mass above the canonical Chandrasekhar mass limit and, hence, the “rotating scenarios” for SNe Ia progen-

* E-mail: amedeo.tornambe@oa-roma.inaf.it (AT), piersanti@oa-abruzzo.inaf.it (LP), raimondo@oa-abruzzo.inaf.it (GR), raffaele.delgrande@oa-roma.inaf.it (RD)

itors allow one to explain the origin of both “normal” and superluminous events, the leading parameter being the total mass of the exploding object. An important consequence of such an evolutionary scenario is that accreting WDs in the mass range $1.4\text{--}2.2^1 M_\odot$ are stable as the pressure gradient is exactly counterbalanced by the effective gravity (gravitational plus “centrifugal” forces), so that they cannot attain the physical conditions suitable for C-ignition in the innermost zone. In order to get such an outcome, it is necessary that the angular velocity profile of the accreting WD is modified either via internal angular momentum distribution, as occurs in differentially rotating objects, or via angular momentum losses. Even if the exact physical characterization of these two processes is still missing it is reasonable to estimate that they need at least several 10^6 yr; during this time span all the information about the original binary systems is lost, so that the only way to find *directly* an imprint of the donor star would be to analyze astronomical frames taken at the Pleistocene Era!

In the present work, we derive expected observational properties of SNe Ia progenitors close to the explosion epoch by assuming that rotation is the leading parameter driving both the mass transfer phase and the evolution up to the Carbon ignition at the center. With this aim we adopt the rotating DD scenario for the progenitors by Piersanti et al. (2003a,b) and we compute full evolutionary models from the onset of the mass transfer process up to the dynamical breakout, which occurs when the temperature at the burning point approaches $\simeq 8 \times 10^8$ K (Lesaffre et al. 2006). We note that our analysis and findings are valid also for the rotating SD scenario as well as for the CD scenario. In fact, when rotation is properly taken into account, the mass transfer process does not directly drive the accreting WD to the explosion, but it continues up and beyond the canonical Chandrasekhar mass limit until the mass reservoir is completely exhausted. After that, the evolution up to the explosion is determined by the angular momentum redistribution along and/or angular momentum losses from the accreted CO WD, independently of the previous evolution. Our analysis is not applicable to the *prompt merging* scenario by Pakmor et al. (2012) as well as to the canonical non-rotating SD scenario.

The present work is structured as follows: in §2 we review the accretion phase in the rotating DD scenario, exploring the dependence of the results on various assumptions about the physical mechanism driving the mass accretion process; in §3 we discuss the physical properties of the WD after the mass accretion has stopped and we analyze its evolution up to the explosion; in §4 we derive the expected observational properties during the last few months before the explosion of the massive WD. Finally, our results are summarized and discussed in §5.

¹ The upper limit is fixed by considering that in the DD scenario the maximum allowed mass for a CO WD is not larger than $1.1 M_\odot$, according to standard stellar evolution. On the other hand, in the SD scenario, due to the partial retention of the accreted matter onto the CO WD, it appears quite unrealistic that the mass of the exploding object could exceed such a limit (see also Hachisu et al. 2012).

2 THE MASS TRANSFER PHASE

In the present computations we use as initial CO WD the same model with total mass $M_{\text{WD}} = 0.8 M_\odot$ as in Piersanti et al. (2003a) and we assume that it is embedded in a close binary system with another CO WD with mass $M_{\text{donor}} = 0.71 M_\odot$. We compute all the evolutionary sequences by using the F.R.A.N.E.C. evolutionary code Chieffi & Straniero (1989), modified according to the prescriptions in Piersanti et al. (2003a,b) to account for the effects of rotation in the hypothesis of high efficiency of angular momentum transport.

Due to gravitational wave radiation (GWR) emission the binary system shrinks and the less massive component first overfills its own Roche lobe, giving rise to a dynamical mass transfer so that it completely disrupts forming a thick accretion disk around the surviving companion. CO-rich matter flows from the disk to the WD at a very high rate, depositing also angular momentum. The rapid mass accretion determines a huge thermal energy excess and produces a large increase of the surface angular velocity, so that the accretor expands on a very short timescale and attains on the surface the critical angular velocity. In this condition, no more matter can be added, so that mass deposition stops for a while and, hence, thermal energy can be diffused inward and the WD can contract. The accretor recedes from the critical conditions and mass deposition can resume. The rate at which matter could be added to the CO WD is determined by its structural properties, in particular by the temperature profile. Later on, when the structure becomes thermally balanced, so that the inward heat transfer timescale becomes longer, the effective accretion rate is determined by other physical mechanisms. In Piersanti et al. (2003b) it has been shown that owing to the continuous angular momentum deposition, the WD increases its rotational energy and, when the latter attains a critical value, the accretor adopts an ellipsoidal shape, so that it acquires a quadrupole momentum and gravitational wave radiation is emitted, thus braking down the WD itself. Several different mechanisms have been suggested by various authors to describe the angular momentum losses from the accreting WD (see e.g. Andersson et al. 1999; Boshkayev et al. 2014; Ilkov & Soker 2012, and references therein). In the present work we do not assume any specific physical mechanism, but we describe such a process as an exponential law by adopting two characteristic timescales, namely $\tau_B = 10^5$ and 10^6 yr as representative of the braking efficiency².

In Figure 1 we report the evolution in the Hertzsprung-Russell (HR) diagram of the models computed with different braking timescales, as labeled. For comparison we report also the model computed by assuming that angular momentum is lost from the accreting WD via gravitational wave radiation emission already discussed in detail in Tornambé & Piersanti (2013). In the figure, we display only the evolution relative to the accretion phase, i.e. up to the point when the total mass stored in the accretion disk has been transferred to the CO WD and its total mass ap-

² The formulation of the braking law is the same as in Piersanti et al. (2003b) - see their Eq. 3 and the corresponding discussion in §4.

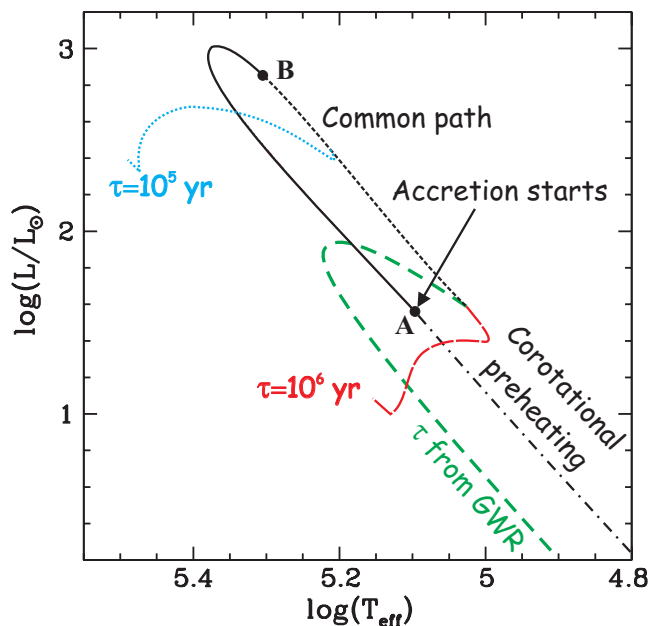


Figure 1. The evolution in the HR diagram of a $0.8 M_{\odot}$ rotating CO WD accreting mass from an accretion disk. The computation has been halted when the WD attains the Chandrasekhar mass limit for rigidly rotating objects. Point **A** marks the onset of mass transfer, while point **B** refers to the epoch when the critical angular velocity is attained on the surface of the accretor. Dotted line refers to the model computed by assuming as braking timescale $\tau_B = 10^5$ yr, while the sequence depicted with a long dashed line have been obtained by fixing $\tau_B = 10^6$ yr. For the sake of comparison we plot also the model computed by Piersanti et al. (2003b), under the assumption that angular momentum is lost via GWR after the accretor has deformed into a Jacobi ellipsoid (heavy dashed line).

proaches the Chandrasekhar mass limit for rigidly rotating degenerate objects.

Figure 1 clearly illustrates that the surface properties of the accreting WD do depend on the angular momentum evolution, as determined by both the mass deposition and the efficiency of the physical mechanism decreasing the angular momentum. In particular, independently of the assumed value for τ_B , after the onset of the “self-regulated” accretion phase at point **A**, all the models follow the same evolutionary path, which is determined only by the inward diffusion of the thermal energy excess produced on the surface by mass deposition during the early phase of mass transfer (from point **A** to **B** in Figure 1). During the “self-regulated” accretion phase the mass transfer rate progressively decreases as the thermal balance along the accreting WD is approached and the evolutionary timescale becomes longer. The following evolution and, hence, the luminosity level at which the accretor starts contracting and evolves blueward depend on the assumed braking efficiency. In particular, the higher the τ_B value, the larger the braking efficiency, the higher the corresponding value of the mass (and angular momentum) deposition rate and, hence, the higher the luminosity level. Figure 1 also shows that for the model having braking efficiency determined by the GWR emission the luminosity of the accretor drops rapidly during the last part of the mass transfer phase, when its total mass is approaching the Chan-

drasekhar mass limit for rigidly rotating degenerate objects. In fact, according to the discussion in §3.3 of Piersanti et al. (2003b), the GWR efficiency drops rapidly, thus determining a rapid reduction of the effective mass transfer rate. As a consequence, the thermal imbalance in the accretor is completely smeared out by thermal diffusion active on a timescale shorter than 10^7 yr, so that the surface luminosity rapidly decreases. Model with $\tau_B = 10^6$ yr exhibits a moderate decrease of the surface luminosity, while that with $\tau_B = 10^5$ yr maintains almost the same luminosity level. According to the previous considerations, in models with high braking efficiencies the thermal energy delivered in the surface layers during the early phase of mass transfer remains locally stored up to the end of the mass deposition phase. This has an important consequence for the expected observational properties during the following evolutionary phase, when the WD attains the physical conditions for carbon ignition in the inner zone where the degeneracy level is very high (see Section 3).

It is worth emphasizing here that once the accretion process ceases, the total mass of the smaller WD has been accreted onto the larger WD leaving no circumstellar material to veil the surface of the remaining WD prior to its explosion.

We note that our results do not depend on the initial mass of the accreting WD, as discussed in Tornambé & Piersanti (2013, see their Figure 5), because at each epoch the evolutionary properties depend only on the assumed efficiency of angular momentum losses, for a fixed value of the total mass of the accretor.

The results discussed above have been obtained assuming high efficiency of angular momentum transport inside the accreting WD, so that the accretor behaves as a rigid rotator. However, the same considerations and results are still valid also when assuming that the angular momentum transport inside the CO WD is a secular process, albeit with some relevant differences. First of all, due to the local storage of the deposited angular momentum in the external layers, the accreting WD attains more rapidly the critical conditions; moreover, as the spinning-up decreases the effective local gravity, the density in the external layers is lower with respect to rigidly rotating degenerate objects and, hence, the compressibility of the zone is higher. As a consequence, when angular momentum transport is treated as a secular process, the surface layers of the accretor heat up at a higher rate, so, as a whole, the evolution in the HR diagram is quite similar to those displayed in Figure 1 (from **A** to **B**), even if the exact luminosity level as well as the corresponding effective temperature at the epoch of the Roche instability (point **B** in Figure 1) depends on the efficiency of angular momentum transport. During the “self-regulated” accretion phase, since a large part of the deposited angular momentum remains localized in the surface layers, the effective mass accretion rate decreases more rapidly with respect to rigidly rotating objects; as a consequence, the evolutionary timescale becomes longer and, hence, angular momentum can be transferred inward efficiently. In fact, the luminosity level at which the accretor starts evolving blueward, is determined by the interplay between angular momentum losses and inward angular momentum transport, which, in turn, determines the exact value of the effective mass accretion rate. According to the previous considerations, we can safely derive that, in-

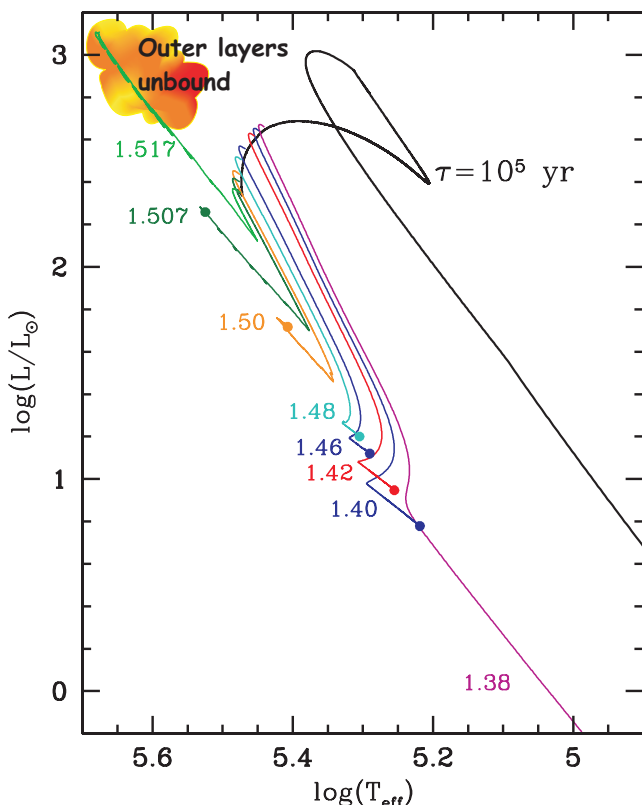


Figure 2. Evolution in the HR diagram of models with different total mass M_F , as labeled, and the same efficiency of angular momentum losses. The evolution refers to the time spanning from the end of the mass transfer process and the epoch of the explosion, marked with a heavy dot.

independently of the angular momentum transport efficiency, the differentially rotating WD attains a lower luminosity for a fixed value of the efficiency of angular momentum losses. Finally, we remark that, since the effective mass transfer rate is lower and, hence, the evolutionary timescale is longer, the thermal energy excess in the external layers is smeared out very rapidly, as for the rigid rotating model losing angular momentum via GWR. The occurrence of the luminosity drop, displayed in Figure 1 for the latter model, could not occur at all because the differentially rotating WD could never reach its own Chandrasekhar mass limit³ during the mass and angular momentum deposition phase.

3 THE FINAL PATH TO THE EXPLOSION

In the framework of the rotating DD scenario, all the available mass constituting the original donor and forming the accretion disk around the accreting CO WD is completely transferred without causing the C-ignition, and, hence, the explosion as SN Ia. In fact, rotation decreases the effective gravity along the whole structure so that a strong gravitational contraction as the total mass increases is avoided.

³ We recall that, depending on the angular velocity profile, the Chandrasekhar mass limit for a differentially rotating degenerate object can exceed $5 M_\odot$.

Therefore, when the mass reservoir has been exhausted the resulting object is a stable massive WD whose further evolution should be a slow and continuous cooling. However, it has been suggested that these massive rotating objects are secularly unstable and, hence, they should lose angular momentum via different physical mechanisms (see, e.g. Andersson et al. 1999; Boshkayev et al. 2014; Ilkov & Soker 2012, and references therein). Owing to the reduction of the total angular momentum, the WD undergoes a strong compression so that it can heat up and ignite carbon in the innermost zones in highly degenerate physical conditions.

To model this phase, once again we adopt an exponentially decaying law for the total angular momentum and we parametrize the angular momentum losses efficiency by using different timescale, as in the previous section. In Figure 2 we report the evolution in the HR diagram of models computed by adopting $\tau_B = 10^5$ yr and different total masses of the initial binary system, as labeled, from the end of the mass transfer process up to the explosion epoch (marked with a dot).

It is worth noticing that, as already recognized (Geroyannis & Papatirou 2000; Boshkayev et al. 2013), when angular momentum is removed from a rigidly rotating degenerate object more massive than the canonical non-rotating Chandrasekhar mass limit, the structure reacts by increasing its rotational velocity. This is clearly shown in Figure 3, where we report the time evolution of the angular velocity for models losing angular momentum with $\tau_B = 10^5$ yr and different total mass, as labeled. Such a behaviour can be easily understood when considering that rotating stars are not solid but gaseous object; as a consequence, when angular momentum is subtracted, the local effective gravity increases and the star reacts contracting to achieve a new hydrostatic equilibrium configuration and, hence, spins up. As a matter of fact, all the models considered in Figure 2 experience an increase of the angular velocity as angular momentum is lost. In any case the value of the critical angular velocity on the surface increases more rapidly than ω so that the structure is gravitationally stable.

As angular momentum continues to be subtracted, WDs with different total mass experience different evolutionary paths. In particular, the model with $M_F = 1.38 M_\odot$ becomes fully supported by the pressure of degenerate electrons and, hence, cannot contract further. Thus, the angular momentum losses remain the only physical process driving the evolution of the angular velocity, which attains a maximum and later on decreases continuously until the WD is practically at rest. Models more massive than $1.39 M_\odot$, but smaller than $1.42 M_\odot$, experience the same evolution even if, owing to the homologous compression of the whole structure, they succeed in igniting carbon before the large part of the star attains highly degenerate physical conditions (see model with $M_F = 1.40 M_\odot$ in Figure 2). Finally, massive WDs contract so rapidly and, hence, heat up so efficiently, that carbon is ignited when the star is still spinning up. The drop in the angular velocity value observed in the final part of the curves corresponding to models with total mass $M_F = 1.40$ and $1.50 M_\odot$ after the accretion process is due to the onset of central convection triggered by the huge energy released via $^{12}\text{C} + ^{12}\text{C}$ reactions.

The evolution of surface properties of the considered

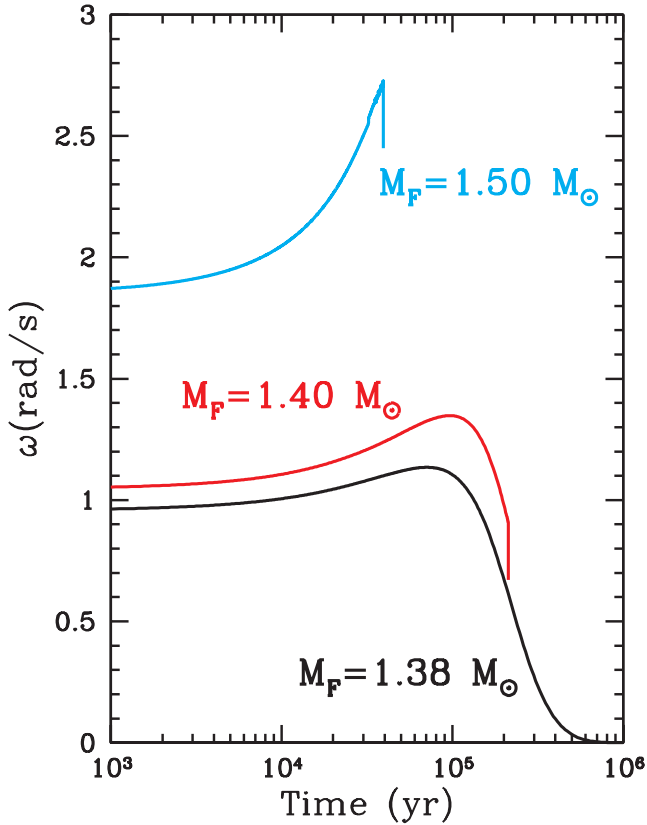


Figure 3. Time evolution of the angular velocity ω for models with different total mass (as labeled), but the same efficiency of angular momentum losses. Time is set arbitrarily to zero at the epoch of the end of mass transfer process.

models after the end of the accretion process and up to the explosion depends mainly on the actual total mass of the accreted WD. In particular, after the mass reservoir is exhausted and the evolution of the WD is driven by the angular momentum loss, all the computed models experience a luminosity drop (see Figure 2). In this phase, owing to the reduction of angular momentum, the accreted WD contracts, heating up via homologous compression. In addition, as the evolutionary timescale becomes longer, the thermal energy excess in the accreted layers determined by the local compression via mass deposition, is efficiently removed via inward thermal diffusion, while plasma neutrino emission efficiently reduces the thermal content of the whole star⁴. In models with total mass lower than $1.50 M_{\odot}$ the thermal diffusion occurs on a timescale shorter than the compressional heating determined by the angular momentum losses, so that the decrease of the surface luminosity continues up to when $^{12}\text{C} + ^{12}\text{C}$ reactions are fully ignited (corresponding to the point with the largest effective temperature in Figure 2). At variance, for larger masses, the luminosity starts to increase before C-burning is ignited at a significant level. This different behaviour is due to the fact that more massive WDs are closer to the rotating Chandrasekhar mass limit; as a consequence, the contraction driven by angular momentum losses triggers a more rapid and, hence, more efficient com-

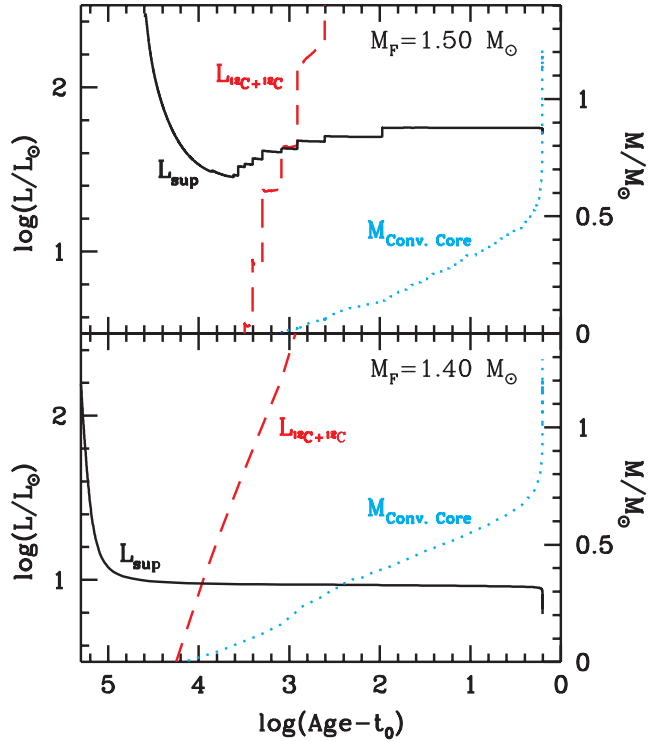


Figure 4. Temporal evolution of the surface luminosity (solid line), of the carbon-burning luminosity (dashed line) and of the mass extension of the convective core (dotted line) for models with total mass $M_F = 1.40$ and $1.50 M_{\odot}$ (lower and upper panel, respectively). Time (in yr) is expressed relative to the epoch of the explosion, which has been set to $t_0 = 2.1198 \times 10^5$ yr and 3.9245×10^4 yr for models in the lower and upper panel, respectively. For both models we assume that angular momentum losses occur on the same timescale, namely $\tau_B = 10^5$ yr.

pressional heating of the whole star, thus determining an increase of the surface luminosity. This occurrence is illustrated in Figure 4 where we report results for models with total mass after accretion $M = 1.40$ and $M = 1.50 M_{\odot}$ (lower and upper panel, respectively) the total surface luminosity (L_{sup} , solid lines), the luminosity produced by carbon fusion reactions ($L_{^{12}\text{C}+^{12}\text{C}}$, dashed lines) and the mass extension of the convective core ($M_{\text{Conv. Core}}$, dotted lines). Figure 4 also shows that the energy (per unit of time) produced via carbon burning at the center triggers very soon the formation of a convective zone which rapidly grows in mass, involving almost 95% of the whole star. This determines a new change in the physical properties of the star, which starts to expand due to the fact that the thermal content in the whole convective region largely deviates from that of a cold fully degenerate object. As a consequence the star expands and, hence, as the evolutionary timescale becomes shorter than the timescale on which angular momentum is removed, the angular velocity starts to decrease (see the sudden drop in the ω profiles for models with total mass $M_F = 1.40$ and $1.50 M_{\odot}$ displayed in Figure 3). This corresponds to the last few days of evolution before the explosion.

In Figure 5 we compare the evolution in the HR diagram of models with the same total mass, namely $1.46 M_{\odot}$ (dotted lines) and $1.50 M_{\odot}$ (dashed lines) but with different efficiency of angular momentum losses after the end of the mass trans-

⁴ Radiative losses are almost negligible in this phase

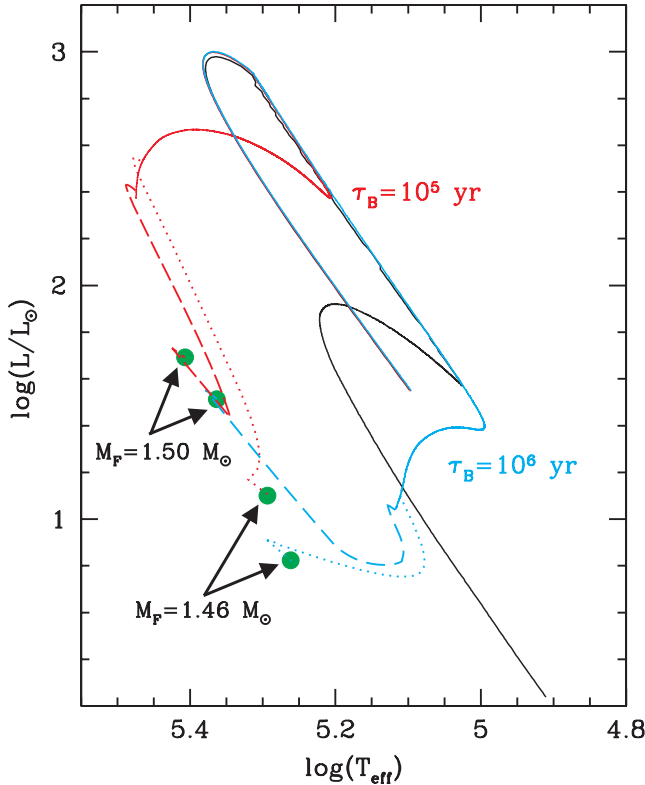


Figure 5. Evolution in the HR diagram of models with the different total mass and efficiency of angular momentum losses.

fer phase. We note that, for a fixed value of the total mass, the surface properties of the exploding objects are quite similar, independently of the timescale adopted to remove angular momentum. Such a finding is confirmed by several other computations performed by varying both M_F and τ_B .

Finally, we note that during the last part of the evolution, when the WD starts to expand due to the large energy injected by C-burning, both ω and the critical angular velocity on the surface decrease, but at a different rate, so that the star remains gravitationally bound. The only model deviating from such a behavior is the one with total mass $M_F = 1.517 M_\odot$. In this case the most external layers experience the Roche instability so that it can be argued that $\simeq 0.01 M_\odot$ of matter has to be lost before the explosion could occur.

4 ABOUT THE OBSERVATIONAL PROPERTIES

In order to compare theoretical models with observational properties of SNe Ia progenitors, we assume genuine black bodies as well as spectral energy distribution (SED) models. To our knowledge, carbon and oxygen model atmospheres of such peculiar WDs do not exist in the extant literature, so we adopt pure-Helium models from the library available in the Tübingen non-local thermodynamic equilibrium (NLTE) Model-Atmosphere Package (TMAP) database⁵ (Rauch & Deetjen 2003; Rauch 2010).

Table 1 lists the theoretical and the corresponding observable values for the set of rotating SNe Ia progenitors considered in the present work at the epoch of the explosion. We provide, for each model, the mass and luminosity (columns 1 and 2, solar units), the effective temperature (column 3, in K), absolute AB magnitudes for the Galex filters FUV and NUV (columns 4 and 5, respectively), the Sloan filters (columns 6–10), two filters of the Advanced Camera for Surveys (ACS) on board of the Hubble Space Telescope (HST), and, finally, the luminosity in two X-ray bands.

We perform the same evaluation by considering NLTE model atmospheres. Synthetic magnitudes in the GALEX, Sloan and ACS photometric bands, as well as for filters in the UVIS and IR channels of the Wide Field and Camera 3 (WFC3) have been calculated using the *iraf* task *calcphot* of STSDAS and calibrated with WDs in the HST database⁶. A selection of magnitudes is reported in Table 2. As it can be easily noticed, pure He models are 0.3 – 0.5 mag fainter than black-body models, the exact value depending on the mass of the exploding object and on the adopted braking efficiency.

The values listed in Table 1 and 2 span the whole range of expected magnitudes for SNe Ia progenitors close to the explosion in the framework of the rotationally-driven scenario discussed in the previous sections. We emphasize again that the results are independent of the assumed scenario for the progenitors (SD, DD, CD scenarios) but they are determined mainly by the total mass of the exploding object and, to a lesser extent, on the physical mechanism driving the braking and/or the angular momentum redistribution during the accretion phase. Inspection of these two tables reveals that the spectral distribution is peaked in the far-UV/soft-X range. Moreover, they also show that the related optical emission would be so weak that only nearby events would be detectable.

5 DISCUSSION AND FINAL REMARKS

The recent observations of SN 2011fe in M 101 (Nugent et al. 2011a,b) and SN 2014J in M 82 (Fossey et al. 2014; Zheng et al. 2014) have stimulated a large debate about the possibility to constrain observationally their progenitor systems.

Several studies have reported observational features and suggested possible progenitor systems (e.g. Li et al. 2011; Kelly et al. 2014; McCully et al. 2014). Observations at different wavelengths have suggested that some progenitor systems associated with the SD scenario have to be ruled out for SN 2011fe, leaving a very limited phase space compatible with the DD scenario and really exotic single degenerate systems (Li et al. 2011; Chomiuk et al. 2012). Optical nebular spectra do not show any evidence for narrow H α emission, supporting again a degenerate companion for SN 2011fe. A pre-explosion frame in the HST archive exhibits the same properties, so that red giants and most helium-star companions can be safely ruled out (Li et al. 2011). By using pre-explosive archival HST images of M 82 from the near-UV to the near-IR, Kelly et al. (2014), excluded for SN 2014J a progenitor system having a bright red giant donor, including

⁵ <http://astro.uni-tuebingen.de/~rauch/>

⁶ <ftp://ftp.stsci.edu/cdbs/currentcalspec/>

Table 1. Expected AB absolute magnitudes in various bands for SNe Ia progenitors just before explosion based on black-body models. The different mass of the considered models are determined by the rotationally-driven accretion mechanism as suggested by Piersanti et al. (2003b). Lines 1–7 refer to models computed by adopting as braking timescale 10^5 yr and displayed in Figure 2, while lines 8–9 are relative to models computed with braking timescale 10^6 yr and displayed in Figure 5.

Mass (M_{\odot})	$\log(\frac{L}{L_{\odot}})$	$\log(T_{\text{eff}})$	FUV	NUV	<i>u</i>	<i>g</i>	<i>r</i>	<i>i</i>	<i>z</i>	F435W	F814W	0.5–2 keV	2–10 keV
$\tau_B = 10^5$ yr													
1.400	0.77	5.22	8.14	8.87	9.78	10.33	10.92	11.32	11.70	10.18	11.48	1.67E+23	6.34E-25
1.420	0.94	5.26	7.98	8.73	9.64	10.20	10.78	11.19	11.57	10.04	11.34	3.91E+24	3.59E-19
1.460	1.11	5.29	7.76	8.51	9.43	10.00	10.58	10.99	11.36	9.83	11.14	3.87E+25	3.79E-15
1.480	1.19	5.31	7.70	8.45	9.38	9.94	10.53	10.94	11.31	9.78	11.09	1.52E+26	1.20E-12
1.490	1.26	5.32	7.59	8.35	9.27	9.84	10.42	10.84	11.21	9.68	10.99	3.17E+26	2.07E-11
1.500	1.71	5.41	7.09	7.87	8.80	9.37	9.96	10.38	10.75	9.21	10.53	8.28E+28	1.29E-01
1.507	2.25	5.52	6.52	7.31	8.26	8.83	9.43	9.84	10.22	8.67	10.00	2.03E+31	4.37E+08
$\tau_B = 10^6$ yr													
1.460	0.83	5.26	8.26	9.00	9.91	10.47	11.06	11.47	11.84	10.32	11.62	3.04E+24	2.79E-19
1.500	1.53	5.36	7.19	7.96	8.89	9.45	10.04	10.50	10.83	9.30	10.60	5.04E+27	9.73E-07

Table 2. AB magnitudes for selected filters as derived from NLTE atmospheres models.

Mass (M_{\odot})	V	FUV	NUV	<i>u</i>	<i>g</i>	<i>r</i>	<i>i</i>	<i>z</i>	F225W	F336W	F475W	F555W	F814W	F110W
$\tau_B = 10^5$ yr														
1.400	11.00	8.40	9.17	10.10	10.66	11.25	11.65	12.03	9.26	9.98	10.69	10.90	11.78	12.51
1.420	10.87	8.27	9.05	10.00	10.54	11.12	11.53	11.90	9.14	9.86	10.57	10.78	11.66	12.38
1.460	10.68	8.08	8.85	9.78	10.35	10.93	11.34	11.71	8.95	9.67	10.38	10.59	11.46	12.18
1.480	10.64	8.04	8.81	9.74	10.31	10.89	11.30	11.67	8.91	9.63	10.34	10.55	11.42	12.14
1.490	10.55	7.94	8.72	9.65	10.21	10.80	11.20	11.57	8.81	9.54	10.24	10.46	11.33	12.05
1.500	10.14	7.54	8.32	9.25	9.81	10.39	10.80	11.16	8.41	9.13	9.84	10.05	10.92	11.64
1.507	9.65	7.04	7.82	8.76	9.32	9.90	10.30	10.67	7.91	8.64	9.35	9.56	10.43	11.14
$\tau_B = 10^6$ yr														
1.460	11.15	8.55	9.33	10.25	10.82	11.40	11.81	12.18	9.42	10.14	10.85	11.06	11.94	12.66
1.500	10.19	7.59	8.37	9.30	9.86	10.44	10.85	11.22	8.46	9.18	9.89	10.10	10.98	11.70

recurrent novae with luminosities comparable to the Galactic prototype symbiotic system RS Oph. According to the available data, these authors also remark that a system consisting of two CO WDs as well as a system made by a CO WD and a main sequence star can not be excluded.

In the framework of the rotationally-driven scenario described in the previous sections, it is not surprising that even in the case of nearby SN 2011fe and SN 2014J the imprint of the progenitor system can not be detected in archival frames. In this regard we note that the SN2011fe progenitor should have a magnitude in ACS/F435W band ~ 38 mag or higher, while the current observational limit is 27.4 mag (Li et al. 2011). Also the largest possible X-ray emission in the 0.5–2 keV band, corresponding to the model with mass $1.507M_{\odot}$ (see Table 1), is several orders of magnitude lower than the upper limit inferred for the SN 2014J by Nielsen et al. (2014). In fact, only SNe Ia progenitors in our own Galaxy may be detectable.

As a final consideration, we note that, according to predictions in Table 1 and 2, models accounting for the effects of rotation exhibit a strong feature in the 0.5–2 keV band, having an expected flux which depends on the total mass of the progenitor. Such a feature is completely missing in standard non-rotating Chandrasekhar mass models of SNe

Ia owing to their lower effective temperature. Such an occurrence is clearly illustrated in Figure 6, where we compare models having $\tau_B = 10^5$ and different total masses with the ZSUN model in Piersanti et al. (2017), obtained by accreting directly CO-rich matter onto an initial $0.817M_{\odot}$ CO WD at $\dot{M}=10^{-7}M_{\odot}\text{yr}^{-1}$, mimicking the evolution of a SD system. For the latter object, the expected flux in the 0.5–2 keV band mass is vanishingly small whereas it becomes appreciable for the more massive models obtained in the framework of the rotationally-driven scenario. As a consequence it seems that the X ray flux, even if small, can be used to assess the role played by rotation in the evolution of SNe Ia progenitors.

ACKNOWLEDGEMENTS

It is a pleasure to thank several colleagues for their advices comments, such as I. Domínguez, C. Badenes, B. Fisher, E. Cappellaro, M. Turatto, J. Isern, S. Benetti, E. Bravo, F. Mannucci, M. Dall’Ora, M. Della Valle, E. Garcia-Berro. We want also to thank the referee, J. Danziger, for his useful comments and suggestions which improve the presentation of our results. This work received partial financial support by INAF–PRIN/2014 (PI G. Clementini). The TheoSSA

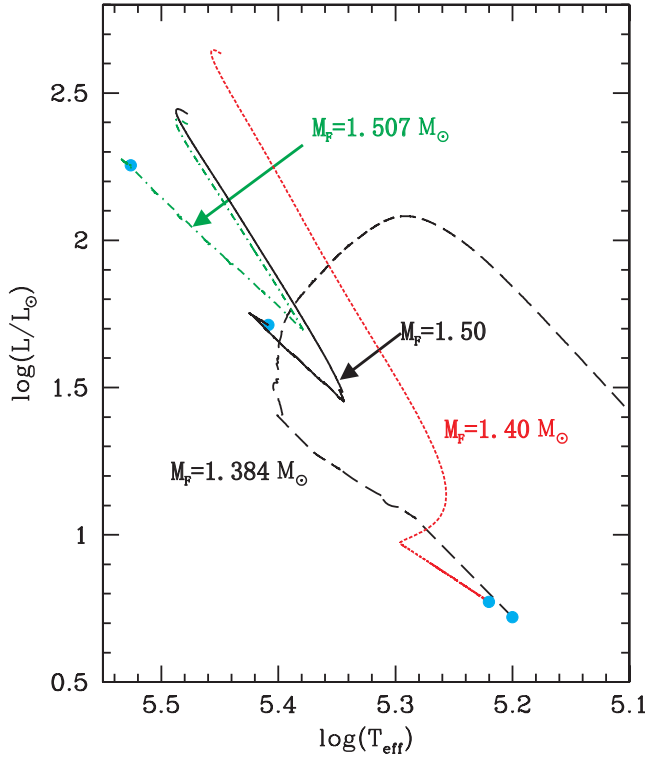


Figure 6. Comparison between a classical non-rotating standard model arising in a Single Degenerate binary system (long dashed line - $M_F = 1.384 M_\odot$) and selected models reported in Figure 2, having $\tau_B = 10^5$ yr and different masses, as labeled.

service (<http://dc.g-vo.org/theossa>) used to retrieve theoretical spectra in this work was constructed as part of the activities of the German Astrophysical Virtual Observatory.

REFERENCES

- Andersson N., Kokkotas K. D., Stergioulas N., 1999, *ApJ*, **516**, 307
- Boshkayev K., Rueda J. A., Ruffini R., Siutsou I., 2013, *ApJ*, **762**, 117
- Boshkayev K., Rueda J. A., Ruffini R., Siutsou I., 2014, *Journal of Korean Physical Society*, **65**, 855
- Chieffi A., Straniero O., 1989, *ApJS*, **71**, 47
- Chomiuk L., et al., 2012, *ApJ*, **750**, 164
- Di Stefano R., Voss R., Claeys J. S. W., 2011, *ApJ*, **738**, L1
- Fossey S. J., Cooke B., Pollack G., Wilde M., Wright T., 2014, *Central Bureau Electronic Telegrams*, **3792**
- Geroyannis V. S., Papasotiriou P. J., 2000, *ApJ*, **534**, 359
- Hachisu I., Kato M., Nomoto K., 2012, *ApJ*, **756**, L4
- Iben Jr. I., Tutukov A. V., 1984, *ApJS*, **54**, 335
- Ilkov M., Soker N., 2012, *MNRAS*, **419**, 1695
- Kelly P. L., et al., 2014, *ApJ*, **790**, 3
- Lesaffre P., Han Z., Tout C. A., Podsiadlowski P., Martin R. G., 2006, *MNRAS*, **368**, 187
- Li W., et al., 2011, *Nature*, **480**, 348
- McCully C., et al., 2014, *Nature*, **512**, 54
- Nielsen M. T. B., Gilfanov M., Bogdán Á., Woods T. E., Nelemans G., 2014, *MNRAS*, **442**, 3400
- Nugent P. E., et al., 2011a, *Nature*, **480**, 344
- Nugent P., Sullivan M., Bersier D., Howell D. A., Thomas R., James P., 2011b, *The Astronomer's Telegram*, **3581**

- Pakmor R., Kromer M., Taubenberger S., Sim S. A., Röpke F. K., Hillebrandt W., 2012, *ApJ*, **747**, L10
- Piersanti L., Gagliardi S., Iben Jr. I., Tornambé A., 2003a, *ApJ*, **583**, 885
- Piersanti L., Gagliardi S., Iben Jr. I., Tornambé A., 2003b, *ApJ*, **598**, 1229
- Piersanti L., Bravo E., Cristallo S., Domínguez I., Straniero O., Tornambé A., Martínez-Pinedo G., 2017, *ApJ*, **836**, L9
- Rauch T., 2010, TheoSSA TMAP Web Interface, VO resource provided by the GAVO Data Center, <http://dc.zah.uni-heidelberg.de/theossa/q/web/info>
- Rauch T., Deetjen J. L., 2003, in Hubeny I., Mihalas D., Werner K., eds, *Astronomical Society of the Pacific Conference Series Vol. 288, Stellar Atmosphere Modeling*. p. 103 ([arXiv:astro-ph/0403239](https://arxiv.org/abs/astro-ph/0403239))
- Tornambé A., Piersanti L., 2013, *MNRAS*, **431**, 1812
- Whelan J., Iben Jr. I., 1973, *ApJ*, **186**, 1007
- Zheng W., et al., 2014, *ApJ*, **783**, L24

This paper has been typeset from a \LaTeX file prepared by the author.